IEEE Photonics Journal
An IEEE Photonics Society Publication

Open Access

# Ultrabroadband and Flattened Dispersion in Aluminum Nitride Slot Waveguides

Volume 9, Number 4, August 2017

**Jiayuan Li**
**Ke Xu**, ***Member, IEEE***
**Jiangbing Du**, ***Member, IEEE***

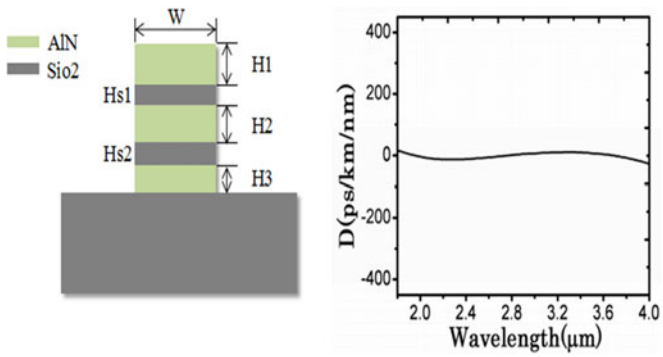


DOI: 10.1109/JPHOT.2017.2716956
1943-0655 © 2017 IEEE

# Ultrabroadband and Flattened Dispersion in Aluminum Nitride Slot Waveguides

**Jiayuan Li,**[1] **Ke Xu,**[1] ***Member, IEEE*,**
**and Jiangbing Du,**[2] ***Member, IEEE***

[1]Department of Electronic and Information Engineering, Shenzhen Graduate School, Harbin Institute of Technology, Shenzhen 518055, China
[2]State Key Laboratory of Advanced Optical Communication Systems and Networks, Shanghai Jiao Tong University, Shanghai 200240, China

*DOI:10.1109/JPHOT.2017.2716956*


Manuscript received May 4, 2017; revised June 2, 2017; accepted June 13, 2017. Date of publication June 19, 2017; date of current version June 29, 2017. This work was supported by NSFC61505039 and Shenzhen Fundamental research projects under the JCYJ20150403161923530. Corresponding author: Ke Xu (e-mail: kxu@hit.edu.cn).

**Abstract:** Aluminum nitride (AlN) is an emerging platform for a wide range of on-chip applications. One promising feature is that both the second- and third-order nonlinearities are available in crystalline AlN waveguides. We design an AlN slot waveguide with a flat and low dispersion over an ultrawide spectral range from near-infrared to mid-infrared. A dual-slot structure is designed and the flattened group velocity dispersion within $-13$ and $+11$ ps/(nm·km) over 2000-nm-wide bandwidth with three zero dispersion wavelengths is achieved. The impacts of the structural parameters are analyzed in detail and the phase-matching condition in four-wave mixing process is investigated as well. A 3-dB conversion bandwidth of 1200 nm and $-28$-dB conversion efficiency are predicted in a 1-cm-long horizontal dual-slot AlN waveguide with the pump power of 2 W.

**Index Terms:** Waveguides, nonlinear optical effects in semiconductors.

## 1. Introduction

As a CMOS compatible material, aluminum nitride (AlN) is a promising system-on-chip platform. It holds excellent properties for optomechanical, electro-optic, and nonlinear applications [1]–[3]. Bulk AlN has a wide bandgap of 6.2 eV that allows for a wide transparent spectral range. High quality AlN film can be deposited on various substrates and the waveguides can be fabricated by mature nano-photonic process. As a result, the AlN waveguides have been reported with low propagation loss from ultraviolet to infrared wavelengths [4]. This allows for the chip scale integration of different types of systems. Silicon is a proven platform for multi-system integration and it exhibits a strong $\chi^{(3)}$ nonlinearity. But it cannot work on visible light and suffers from two photon absorption at the near-infrared (IR) region. Most importantly, the $\chi^{(2)}$ effect is intrinsically not available in silicon. AlN is one of the materials that possess both second and third order nonlinearity. Thus it enables the monolithic integration of the two types nonlinear optical circuits.

The AlN optical nonlinear waveguides have been extensively studied for frequency conversion and comb generation from visible light to infrared region [5]–[7]. The frequency conversion enabled by $\chi^{(2)}$ can be easily achieved in the phase-matched AlN waveguides. The third order nonlinearity of AlN is an alternative and a more flexible way to achieve wavelength conversion through

four wave mixing (FWM). The distinct feature of this material is that the frequency comb over a wide bandwidth can be generated due to its wide operation window. The $\chi^{(3)}$ nonlinearity has a more critical requirement on dispersion control. Broadband low dispersion is usually desired to ensure the phase matching condition over a wide wave band. Besides, the low dispersion avoids pulse broadening and compression which leads to signal distortion. The dispersion engineering is thus essential for signal transmission as well. The dispersion engineered AlN waveguides with optimized cross-section aspect ratios have been demonstrated for comb generation based on cascaded four-wave mixing [5]. However, the reported bandwidth is limited to a few hundreds of nanometers in the near-IR. This is because the dispersive properties are not that sensitive to the geometry change for the AlN waveguides which have relatively weak optical confinement. In addition to modifying the aspect ratio, adding a low-index cap layer to the waveguide core is another way to flatten the dispersion in a high-index material like silicon [8]. But this technique does not work well for the low-index core material. A third method to realize broadband low dispersion is based on slot waveguides [9]. A silicon slot waveguide was demonstrated with a flat dispersion of $0 \pm 16$ ps/(nm·km) over 553 nm wavelength range [10]. Then a flattened dispersion over 670 nm bandwidth was obtained from $-22$ to $+20$ ps/(nm·km) with four zero dispersion wavelengths (ZDWs) in a silicon slot waveguide [11].

It is known that mid-IR photonics have a wide range of applications like sensing, communications, spectroscopy and so on but the available laser sources in this wide spectrum are very limited. The generation of new frequencies through nonlinear process is thus important. The study of dispersion engineering in AlN waveguides in this wavelength range will be helpful to achieve efficient nonlinear optical applications on integrated platform. In this paper, we tailor the dispersion of the AlN slot waveguides from near-IR to mid-IR. The horizontal single-slot waveguides are studied first and a flat dispersion profile between $-12$ and $+15$ ps/(nm·km) over 1250 nm bandwidth is achieved. Then the horizontal dual-slot structures are investigated and a record broadband low dispersion between $-13$ and $+11$ ps/(nm·km) is achieved over 2000 nm wavelength range. This is the broadest low dispersion achieved in AlN waveguides according to our best knowledge. Then the phase-matching condition in the dual-slot waveguide is studied as well. An ultra-width conversion bandwidth of 1200 nm is achieved with $-28$ dB conversion efficiency based on degenerate FWM progress.

## 2. Waveguide Structures and Dispersion Profiles

The vertical slot waveguide can guide TE mode well in a wide wavelength range while TM mode can be well-guided in a horizontal slot waveguide [12]. Fig. 1(a) and (b) are schematic diagrams that depict the AlN waveguides with a horizontal single-slot and vertical single-slot, respectively. The slot material is silicon oxide which can be either thermally grown or deposited by plasma-enhanced chemical vapor deposition (PECVD). The slot is sandwiched between two AlN layers, and the substrate is 3-$\mu$m oxide. The slot optical mode can be strongly confined in the slot region due to the discontinuity of the electric field at the interfaces between the strip and slot [9]. We calculate the effective index (EI) of different wavelengths by using finite-element method (FEM). The convergence condition of the FEM mode solver is controlled by a relative tolerance parameter which is the relative error in the computed eigenvalues. Here we set it to be $10^{-8}$. The material dispersion of AlN and $SiO_2$ are obtained from [13]. Then the group velocity dispersion (GVD) can be calculated by:

$$D = -(\lambda/c) \cdot (\partial^2 n\text{eff}/\partial\lambda^2) \tag{1}$$

After carefully tuning the structural parameters of the horizontal single-slot waveguide, a dispersion curve is achieved with three ZDWs indicated by the black line in Fig. 1(c). A flat dispersion profile is obtained when the slot height (Hs), upper AlN layer height (H1), lower AlN layer height (H2) and waveguide width (W) are set to be 202, 1000, 640 and 1576 nm, respectively. The GVD is within 12 and $+15$ ps/(nm km) over 1250 nm bandwidth, from 2.05 $\mu$m to 3.3 $\mu$m. The three ZDWs are located at 2165, 2720, 3175 nm. The red line in Fig 1(c) shows the dispersion profile of vertical single-slot waveguide. We found that the asymmetric structure gave us a better disper-

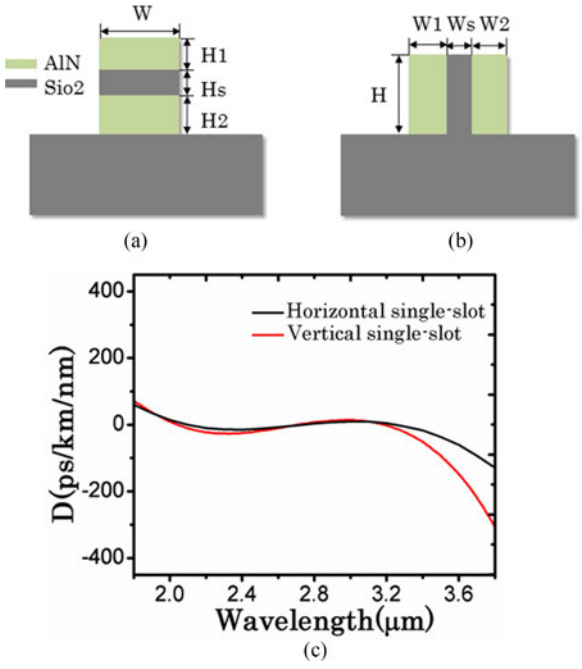


Fig. 1. (a) Horizontal single-slot AlN waveguide structure. (b) Vertical single-slot AlN waveguide structure. (c) Dispersion profiles of horizontal and vertical single-slot waveguides.

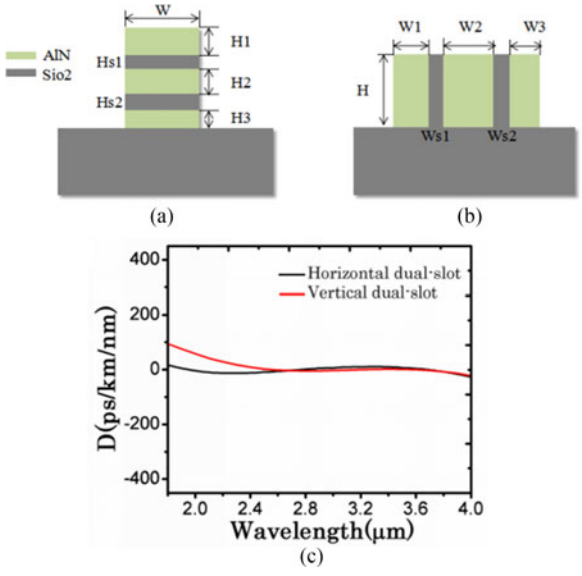


Fig. 2. (a) Horizontal dual-slot AlN waveguide structure. (b) Vertical dual-slot AlN waveguide. (c) Dispersion profiles of horizontal and vertical dual-slot waveguides.

sion profile which is consistent with the results in [14]. The corresponding structural parameters are: W1 = 600 nm, Ws = 202 nm, W2 = 1000 nm, H = 1576 nm. From the result, the dispersion flatness and bandwidth is a bit worse than the horizontal structure.

In order to get a broader, flatter and lower dispersion profile, a dual-slot structure can be used. The schematic diagrams and the parameter descriptions of the proposed dual-slot AlN waveguides are shown in Fig. 2(a) and (b). It is worth noted that the fabrication of the horizontal/vertical waveguides with single or double slot can be possibly realized by standard lithography, etching, deposition and

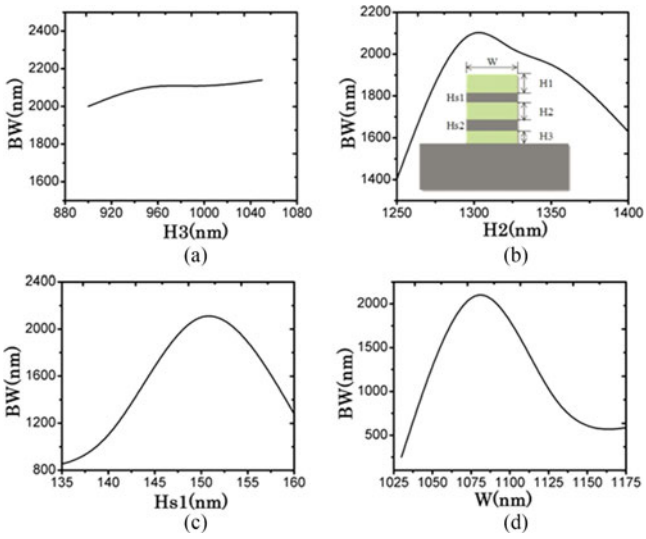


Fig. 3. The defined FOM (bandwidth with a GVD below $\pm$15 ps/nm/km) as a function of (a) H3; (b) H2; (c) Hs1; (d) W.

lift-off process. Similar to the previous method shown above, we calculate the dispersion of quasi-TM mode in horizontal dual-slot and quasi-TE mode in vertical dual-slot waveguide. The dispersion curves of the two structures are plotted in Fig. 2(c). Through numerous simulations and structural parameters tuning, we set the waveguide parameters as follows: the height of upper and lower cladding layer (H1 and H3) is 950 nm, the height of central AlN layer (H2) is 1300 nm, the two sandwiched slot heights (Hs1 and Hs2) is set to be150 nm, and the AlN width waveguide (w) is 1080 nm. We determine these parameters by evaluating a figure of merit (FOM) defined as the bandwidth with a GVD below $\pm$15 ps/nm/km. The FOM dependences on the structural parameters are depicted in Fig. 3. With this structure, we obtain an ultra-flat and low dispersion profile over an ultra-wide bandwidth indicated by the black line in Fig. 2(c). The GVD is between $-13$ and $+11$ ps/(nm km) over 2000 nm bandwidth from 1.85 to 3.85 $\mu$m. There are three ZDWs located at 1956, 2770, 3680 nm, respectively. In vertical dual-slot waveguide, a broad and flat dispersion curve is achieved with width of the left AlN stripe (W1), middle AlN stripe (W2), right AlN stripe (W3) of 550, 1400, 750 nm, respectively. The width of the two slots (Ws1 and Ws2) are 200 nm and the waveguide height (H) is 1180 nm. The resulted dispersion profile is shown by the red line in Fig. 2(c). The bandwidth is much smaller than the horizontal structure.

Comparing the four structures above, we find that all of them can achieve very low and flat dispersion while the bandwidth is different. The dual-slot structure has much broader bandwidth than the single slot and the horizontal structure has slightly better dispersion than the vertical one. As a result, we focus our discussion on how to optimize the horizontal dual-slot AlN waveguide in the following section. In general, the process begins with a set of structure parameters that we think are reasonable. The dependence of the dispersion properties on each structural parameter is investigated by tuning each parameter independently. Then a desired dispersion profile is obtained by adjusting all the structural parameters according to the knowledge of their influence on the dispersion. Fig. 4 shows modal distributions at four different wavelengths, 1400, 2500, 3300, 4500 nm in the horizontal dual-slot waveguide. The optical field is mainly concentrated in the center AlN layer at short wavelengths which is the so called quasi-strip mode. Increasing the wavelength, the hybrid mode is present where most of the field is distributed in the silica and AlN layer. At longer wavelengths, the optical field is gradually transferred into the two slots which is called quasi-slot mode.

Different from standard strip/rib waveguide, the dual-slot waveguide supports different modes over a wide spectral range. The strip mode at short wavelength and the slot mode at long wavelength

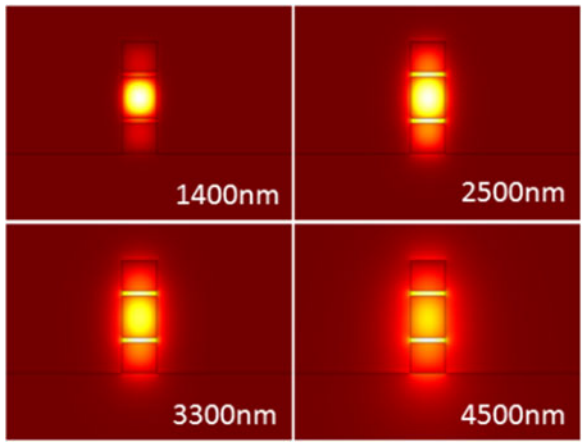


Fig. 4. Quasi-TM mode evolution at different wavelengths in the horizontal dual-slot AlN waveguide.

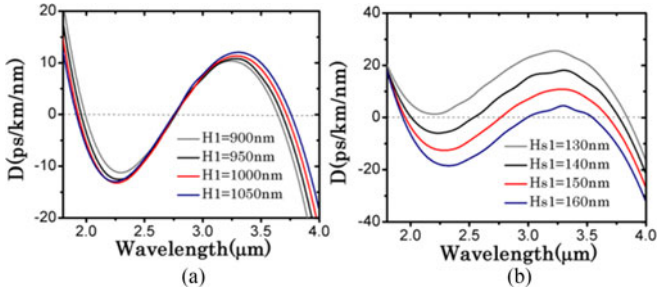


Fig. 5. Dispersion profiles of dual-slot waveguide change with different (a) height of upper AlN layer, (b) height of upper slot.

have significantly different waveguide dispersion properties which allows for the material dispersion compensation with a proper structure. The dispersion engineering of the dual-slot waveguide is realized by carefully choosing the parameters depicted in Fig. 2(a). A flat dispersion over a wide spectral range is achieved via intensive numerical simulations. To study the impact of structural parameters on the dispersion, we fine tune the parameters from the previously mentioned structure that gives a flat and broad dispersion.

Firstly, we vary the height of the upper AlN layer (H1) from 900 to 1050 nm and the GVD curves are plotted in Fig. 5(a). The dispersion has slightly difference under different H1 values but not significant. This is because very limited amount of energy is in this layer. It is a trivial trade-off between the bandwidth and the flatness. Here we choose the optimum value to be 950 nm. The lower AlN layer (H3) has very similar impact on the dispersion as the upper layer. Then, we study how the upper slot height (Hs1) affects the dispersion profile and the results are shown in Fig. 5(b). As the height increases from 130 nm to 160 nm, the dispersion profile is shifted from anomalous to normal dispersion regime. It is a similar trend in dispersion profile with the height of lower slot (Hs2) increased. This waveguide has more sensitivities to the variations of two slots, so we can adjust their heights to realize flatter dispersion.

At short wavelengths, most of the light is confined within the central AlN strip as a quase-strip mode. Thus the dispersion is sensitive to the central AlN dimensions which are AlN height (H2) and waveguide width (w). When the height increases from 1250 nm to 1400 nm, the dispersion profile at short wavelength is significantly changed while the long wavelength dispersion is not affected due to the strip to slot mode conversion. As shown in Fig. 6(a), the optimum dispersion curve is achieved when the central layer AlN height is 1300 nm. Fig. 6(b) shows that the dispersion at long wavelength is markedly changed with different waveguide width. With smaller width, it introduces a large negative GVD and shifts the dispersion curve downwards. From the result, we choose an

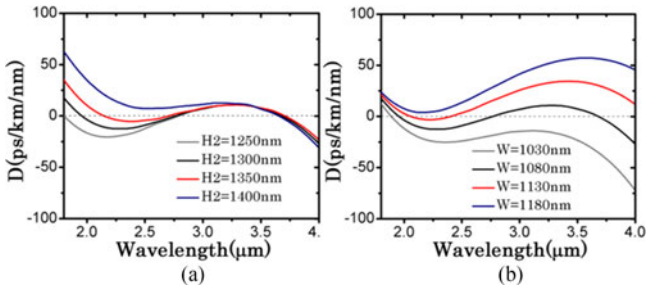


Fig. 6. Dispersion profiles of dual-slot waveguide change with different (a) height of central AlN strip, (b) waveguide width.

optimum waveguide width to be 1000 nm. Fig. 6 reveals that the dispersion properties at short and long wavelength regime can be controlled by different parameters without affecting each other too much.

## 3. Wavelength Conversion

With such a horizontal dual-slot AlN waveguide, we have achieved a broad and flat low dispersion. This allows for efficient FWM which is a phase sensitive nonlinear process. To achieve effective wavelength conversion through FWM, it is important to minimize the phase mismatch. The linear phase mismatch is related to the dispersion profile and the phase mismatch can be expressed by $\Delta\beta = \beta_s + \beta_i - 2\beta_p$, where $\beta_{s,i,p}$ are the wavenumbers of the signal, idler, pump waves, respectively. The $\Delta\beta$ can be rewritten as [15]:

$$\Delta\beta = \beta_2(\omega_p)\Delta\omega^2 + \frac{1}{12}\beta_4(\omega_p)\Delta\omega^4 \tag{2}$$

where $\Delta\omega = \omega_s - \omega_p$ is the frequency difference between the signal and the pump waves, $\beta_2$, $\beta_4$ are the second and fourth order dispersion, respectively.

Wavelength conversion based on third order nonlinearity is an important application that is rarely studied in AlN waveguide. The pump, signal, idler waves are assumed to be quasi-TM mode in our simulation. The coupled equations for the degenerate FWM can be described without the two photon absorption (TPA) and the TPA-induced free-carrier absorption (FCA) terms. Because the nonlinear absorption coefficients are quite small and the even the defect sate absorption edge is far from the mid-IR wavelengths [16].

$$\frac{dA_P(z)}{dz} = -\frac{\alpha_p}{2}A_p(z) + j\gamma_p\left|A_p(z)\right|^2 A_p(z) + 2j\gamma_p\left[\left|A_s(z)\right|^2 + \left|A_i(z)\right|^2\right]A_p(z) + 2j\gamma_p A_p^*(z)A_s(z)A_i(z)\exp(j\Delta\beta z), \tag{3}$$

$$\frac{dA_s(z)}{dz} = -\frac{\alpha_s}{2}A_s(z) + j\gamma_s\left|A_s(z)\right|^2 A_s(z) + 2j\gamma_s\left[\left|A_p(z)\right|^2 + \left|A_i(z)\right|^2\right]A_s(z) + j\gamma_s A_p^2(z)A_i^*(z)\exp(-j\Delta\beta z), \tag{4}$$

$$\frac{dA_i(z)}{dz} = -\frac{\alpha_i}{2}A_i(z) + j\gamma_i\left|A_i(z)\right|^2 A_i(z) + 2j\gamma_i\left[\left|A_p(z)\right|^2 + \left|A_s(z)\right|^2\right]A_i(z) + j\gamma_i A_p^2(z)A_s^*(z)\exp(-j\Delta\beta z), \tag{5}$$

where $A_{p,s,i}$ are the amplitudes of the pump, signal, idler waves respectively and $z$ is the propagation distance. The three equations have similar forms, and the first term of the right-hand side of the (3) represents the linear loss of the waveguide. We use $\alpha_{p,s,i}$ as the linear loss coefficients and can be calculated by $\alpha = 10\log(e^{2\Delta n \cdot k \cdot l})$, where $k$ is wave vector, $\Delta n$ is the imaginary part of efficient index. When the pump wavelength is 1950 nm, the linear loss coefficient is about 1.03 dB/cm which is

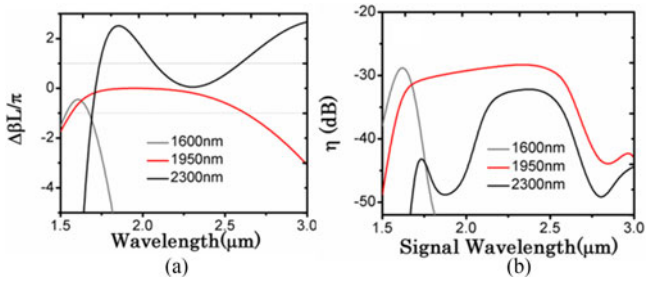


Fig. 7. (a) Linear phase mismatch. (b) Conversion efficiency ($\eta$) at 1600, 1950, 230 nm pump wavelengths in the horizontal dual-slot AlN waveguide.

the simulated value including the radiation loss and the material absorption loss. This value is not underestimated too much since a low loss waveguide loss has been reported experimentally in [4]. The second term shows the self-phase modulation. The $\gamma_{p,s,i}$ are the nonlinear coefficients, where $\gamma = 2\pi n_2/(\lambda A_{\text{eff}})$, $n_2 = 3.8 \times 10^{-19}$ m$^2$/W [5]. The effective mode area is 0.71 $\mu$m$^2$ at 1950 nm. The third term is the cross-phase modulation among three waves. The last term represents nonlinear energy transfer during the process of degenerate FWM. With the parameters calculated above, the evolutions of the wave amplitudes (pump, probe, idler) along the wave propagation are calculated. The step size dz is sufficiently small to ensure the calculation precision. The conversion efficiency can be expressed as $\eta = 10\log(P_{i-out}/P_{s-in})$. Fig. 7(a) shows the linear phase mismatch at three different pump wavelengths in a 1 cm-long horizontal dual-slot AlN waveguide. When the pump wavelength is 1950 nm near a ZDW, a small linear phase mismatch can be obtained over a broad spectral range. Fig. 7(b) is the conversion efficiency with the pump waves located at different wavelengths. A CW pump with the power of 2 W and a signal with the power of 0.1 W are used in the simulation. It can be seen that when the pump wavelengths are located at 1600, 1950, 2300 nm, the 3-dB conversion bandwidth are 300, 1200, 800 nm, respectively. Thus we have achieved $-28$ dB conversion efficiency over an ultra-broad bandwidth at 1950 nm.

## 4. Conclusion

In this paper, a flattened and low dispersion over an ultra-wide band in AlN waveguides is achieved. We have investigated the dispersion engineering in several types of slot structures. With the horizontal dual-slot waveguides, we obtain a dispersion between $-13$ and $+11$ ps/(nm·km) over 2000 nm spectral range with three ZDWs. In addition, we have studied phase matching condition in our proposed waveguide structure. A small phase mismatch can be achieved using pump wavelength near the first ZDW in the proposed dual-slot AlN waveguide. A large conversion bandwidth of 1200 nm is obtained in a 1 cm-long waveguide using a CW pump power of 2 W based on degenerate FWM progress.

## Reference

[1] C. Xiong *et al.*, "Aluminum nitride as a new material for chip-scale optomechanics and nonlinear optics," *New J. Phys.*, vol. 14, no. 9, p. 095014, Sep. 2012.
[2] H. Jung, R. Stoll, D. Fischer, and H. X. Tang, "Green, red, and IR frequency comb line generation from single IR pump in AlN microring resonator," *Optica*. vol. 1, no. 6, pp. 396–399, Dec. 2014.
[3] W. H. P. Pernice, C. Xiong, C. Schuck, and H. X. Tang, "Second harmonic generation in phase matched aluminum nitride waveguides and micro-ring resonators," *Appl. Phys. Lett.*, vol. 100, no. 22, p. 223501, May 2012.
[4] P. T. Lin, H. Jung, L. C. Kimerling, and H. X. Tang, "Low-loss aluminium nitride thin film for mid-infrared microphotonics," *Laser Photonics Rev.*, vol. 8, no. 2, pp. L23–L28, 2014.
[5] H. Jung, C. Xiong, K. Y. Fong, X. Zhang, and H. X. Tang, "Optical frequency comb generation from aluminum nitride microring resonator," *Op.t Lett.*, vol. 38, no. 15, pp. 2810–2813, Jul. 2013.
[6] D. Blanc, A. M. Bouchoux, C. Plumereau, A. Cachard, and J. F. Roux, "Phase-matched frequency doubling in an aluminum nitride waveguide with a tunable laser source," *Appl. Phys. Lett.* vol. 66, no. 6, pp. 659–661, Nov. 1994.

[7] X. Guo, C. L. Zou, and H. X. Tang, "Second-harmonic generation in aluminum nitride microrings with 2500%/W conversion efficiency," *Optica*. vol. 3, no. 10, pp. 1126–1131, Oct. 2016.
[8] Y. Yue, L. Zhang, H. Huang, R. G. Beausoleil, and A. E. Willner, "Silicon-on-nitride waveguide with ultralow dispersion over an octave-spanning mid-infrared wavelength range," *IEEE Photonics J.*, vol. 4, no. 1, pp. 126–132, Feb. 2012.
[9] V. R. Almeida, Q. Xu, C. A. Barrios, and M. Lipson, "Guiding and confining light in void nanostructure," *Opt. Lett.*, vol. 19, no. 11, pp. 1209–1211, Jan. 2004.
[10] L. Zhang, Y. Yue, R. G. Beausoleil, and A. E. Willner, "Flattened dispersion in silicon slot waveguides," *Opt. Exp.*, vol. 18, no. 19, pp. 20529–20534, Sep. 2010.
[11] L. Zhang, Q. Lin, Y. Yue, Y. Yan, R. G. Beausoleil, and A. E. Willner, "Silicon waveguide with four zero-dispersion wavelengths and its application in on-chip octave-spanning supercontinuum generation," *Opt. Exp.*, vol. 20, no. 2, pp. 1685–1690. Jan. 2012.
[12] G. P. Agrawal, *Nonlinear Fiber Optics*. Boston, MA, USA: Academic, 1989.
[13] M. J. Weber, *Handbook of Optical Material*. Boca Raton, FL, USA: CRC Press, 2002.
[14] M. Zhu *et al.*, "Ultrabroadband flat dispersion tailoring of dual-slot silicon waveguides," *Opt. Exp.*, vol. 20, no. 14, pp. 15899–15907, 2012.
[15] X. Zhang, S. Gao, and S. He, "Optimal design of a silicon-on-insulator nanowire waveguide for broadband wavelength conversion," *Progress Electromagn. Res.*, vol. 89, pp. 183–198, 2009.
[16] H. Demiryont, L. Thompson, and G. Collins, "Optical properties of aluminium oxynitrides deposited by laser-assisted CVD," *Appl. Opt.*, vol. 25, no. 8, pp. 1311–1318, 1986.